Testing a maximum evaporation theory over saturated land: Implications for potential evaporation estimation

Zhuoyi Tu[1], Yuting Yang[1], Michael L. Roderick[2]

5 [1]State Key Laboratory of Hydroscience and Engineering, Department of Hydraulic Engineering, Tsinghua University, Beijing, China

[2]Research School of Earth Sciences, Australian National University, Canberra, ACT, Australia

Correspondence to: Yuting Yang (yuting_yang@tsinghua.edu.cn)

Abstract. State-of-the-art evaporation models usually assume the net radiation (R_n) and surface temperature (T_s; or near-surface air temperature) to be independent forcings on evaporation. However, R_n depends directly on T_s via outgoing longwave radiation and this creates a physical coupling between R_n and T_s that extends to evaporation. In this study, we test a maximum evaporation theory originally developed for global ocean over saturated land surfaces, which explicitly acknowledges the interactions between radiation, T_s and evaporation. Similar to the ocean surface, we find a maximum evaporation (LE_{max}) emerges over saturated land that represents a generic trade-off between a lower R_n and a higher evaporation fraction as T_s increases. Compared with flux site observations at the daily scale, we show that LE_{max} corresponds well to observed evaporation under non-water-limited conditions and that the T_s at which LE_{max} occurs also corresponds with the observed T_s. Our results suggest that saturated land surfaces behave essentially the same as ocean surfaces at time scales longer than a day and further imply that the maximum evaporation concept is a natural attribute of saturated land surfaces, which can be the basis of a new approach to estimating evaporation.

1 Introduction

Potential evaporation (E_P), defined as the rate of evaporation (E) that would occur under non-water-stressed conditions, determines the upper boundary of E over a specific land surface for a given meteorological forcing. Although E_P is more of a hypothetical variable and is generally very difficult to observe, it is often the starting point for partitioning rainfall between E, runoff, and soil moisture changes in hydrological, agricultural, ecological and other related studies (Maes et al., 2019; Milly and Dunne, 2016; Scheff and Frierson, 2014; Schellekens et al., 2017; Sheffield et al., 2012; Vicente-Serrano et al., 2013; Wang and Dickinson, 2012). Over the years, numerous mathematical models have been proposed with varying structures and complexities to quantify E_P (e.g., Allen et al., 1998; Priestley and Taylor, 1972; Penman, 1948; Shuttleworth, 1993; Thornthwaite, 1948). Among them, the Penman-Monteith type models (e.g., either the Open Water Penman model (Shuttleworth, 1993) or the Food and Agriculture Organization Penman-Monteith model (Allen et al., 1998)) are most widely used, given their explicit consideration of the radiative and aerodynamic components of E, and are hence generally considered as a physical-based and accurate approximation of the real E processes.

Nevertheless, recent empirical evidence shows that the Penman-Monteith type models perform unsatisfactorily in estimating E_P compared with eddy-covariance observations (i.e., the observed E under non-water-stressed conditions; Maes et al., 2019). Instead, the energy balance-based approaches

40 work better in reproducing E_P in both observations (Maes et al., 2019) and climate model simulations (Milly and Dunne, 2016). From an energy balance point of view, the magnitude of E (or in its energy form – latent heat flux or LE) is determined by the energy balance equation,

$$LE = (R_n - G)\frac{1}{1+\beta} \tag{1}$$

with R_n the net radiation (W m^{-2}) and G the ground heat flux (W m^{-2}), which is often negligibly small

45 over land for time scales longer than a day. In Eq. (1), β is the Bowen ratio and represents the ratio of sensible heat flux (H) over LE (Bowen 1926). As a result, LE is determined by the available energy at the evaporating surface (i.e., $R_n - G$) and the ability of that evaporating surface to convert the available energy into LE, which is represented by the $1/(1+\beta)$ term and often known as the evaporative fraction. With no restriction on water supply, β is known to be a decreasing function of temperature at the

50 evaporating surface (T_s) (Aminzadeh et al., 2016; Andreas et al., 2013; Guo et al., 2015; Philip, 1987; Priestley and Taylor, 1972; Slatyer and McIlroy, 1961; Yang and Roderick, 2019). This implies that when water is not limiting, both T_s and the available energy determine the rate of E. Hence, with fixed available energy, a higher T_s corresponds to a lower β (or a higher evaporative fraction) and therefore a larger LE. This line of reasoning has directly led to the development of energy balance-based

55 evaporation models, including the classic Equilibrium evaporation approach (Slatyer and McIlroy, 1961) and the Priestley-Taylor evaporation model (Priestley and Taylor, 1972). Compared with Penman-Monteith type models, the energy balance-based approach simplifies the representation of the aerodynamic component of E and usually takes the aerodynamic component of E as a fixed fraction of its radiative counterpart (e.g., 0.26 in the Priestley-Taylor model).

60 However, a key issue in the above energy balance-based approach is that it takes R_n to be an independent forcing of E. A similar idea was also adopted in Penman-Monteith type models (Penman, 1948; Monteith, 1965). Nevertheless, it is clear that R_n cannot be physically independent of either E or T_s. On one hand, a higher T_s corresponds to a higher outgoing longwave radiation and therefore a lower

R_n. On the other hand, a higher E is associated with a larger evaporative cooling, which lowers T_s and

65   ultimately feedbacks to R_n. This latter process confirms that T_s is not independent of E. Consequently, the intrinsic interdependence between R_n, E and T_s has long been ignored in the state-of-art evaporation models that require R_n as model input (Yang and Roderick, 2019).

To deal with the above issue, a recent study by Yang and Roderick (2019) explicitly considered the interdependence between radiation, T_s and evaporation and tested the new approach over global ocean

70   surfaces. They found that with the increase of T_s, R_n decreases while evaporative fraction increases (since β decreases as T_s increases) in agreement with a number of previous studies (Aminzadeh et al., 2016; Andreas et al., 2013; Guo et al., 2015; Philip, 1987; Priestley and Taylor, 1972; Slatyer and McIlroy, 1961; Yang and Roderick, 2019). This generic and explicit trade-off between a lower R_n and a higher evaporative fraction with the increase of T_s directly yields a maximum evaporation along the T_s

75   gradient according to Eq. (1) (Yang and Roderick, 2019, also see Sect. 2.2). This maximum evaporation emerges naturally from the R_n-T_s-E interactions and does not require a priori knowledge of T_s thereby alleviating the need for the assumption that R_n and T_s are independent of E in traditional evaporation models. As a result, the maximum evaporation theory does not consider R_n to be an independent forcing of E. Instead, it only requires the ultimate external forcing (i.e., solar radiation) and an assumption that

80   β decreases with the increase of T_s (see Sect. 2.2). Compared with observations of ocean surface evaporation and temperature, Yang and Roderick (2019) demonstrated the validity of the maximum evaporation theory over global ocean surfaces. Here, we test this new maximum evaporation theory over land by asking and answering two questions: does the theory recover the (i) observed E and (ii) does it recover the observed T_s? By recovering, we mean that the maximum E as per theory corresponds

85   to the observed E and the T_s at which the maximum E occurs corresponds to the observed T_s under non-water-stressed conditions. Testing the maximum evaporation theory over land is important, as it determines whether saturated land behaves like the ocean surface and whether the maximum evaporation theory can be the basis of a new approach to estimating E_P over land.

2 Materials and methods

2.1 Flux site observations

Observations of daily actual evaporation (or latent heat flux), sensible heat flux, ground heat flux along with relevant meteorological variables, radiative fluxes and soil moisture were originally obtained from 212 flux sites collected in the FLUXNET2015 database (http://fluxnet.fluxdata.org/data/fluxnet2015-dataset/). Only days with the data quality metric for *LE* and *H* higher than 0.9 (on a scale of 0-1) were used. The daily scale variables were obtained based on 15-min/30min observations using the standard approach (Pastorello et al., 2015). The residual approach (i.e., assuming the observed *H* is correct and *LE* is considered as the residual of the energy balance equation) was used to recalculate the fluxes based on a forced energy balance closure at each flux site (Ershadi et al., 2014). Surface temperature for each site-day combination was calculated based on the observed longwave radiation following:

$$T_s = \sqrt[4]{\frac{R_{lo} - (1-\varepsilon)R_{li}}{\varepsilon\sigma}} \qquad (2)$$

where R_{lo} and R_{li} are respectively the outgoing and incoming longwave radiation, σ is the Stefan-Boltzmann constant (5.67×10^{-8} W m^{-2} K^{-4}) and ε is the surface emissivity, which is acquired from the MODIS (Moderate Resolution Imaging Spectroradiometer) emissivity product (i.e., MOD11A1 Version 6; https://lpdaac.usgs.gov/products/mod11a1v006).

To select a subset of observations at each flux site in which the actual evaporation is not limited by water availability, the energy balance criterion and the soil moisture criterion used by Maes et al (2019) were adopted. Specifically, at each flux site, the evaporative fraction *EF* (i.e., *EF=LE/(LE+H)*) was first calculated and the unstressed measurements consisted of all days with *EF* exceeding the 95th percentile *EF* threshold at each site. Following that, we removed days with soil moisture (averaged over all measured depths) lower than 50% of the maximum soil moisture (taken to be the soil moisture at the 98th percentile) at each site. Finally, any remaining site-days with daily *EF* lower than 0.6 were also removed. To avoid dealing with strongly advective conditions, we additionally removed days having a negative *H* value. As a result, a total of 1128 non-water-stressed site-days from 86 sites passed the above criterion and were used in this study (Figure 1 and Supplementary Table S1).

2.2 The maximum evaporation model

The maximum evaporation model calculates evaporation from a wet surface based essentially on surface energy balance (Eq. (1)) with R_n and β both explicitly represented as functions of T_s (Yang and Roderick, 2019):

$$LE = \frac{R_n(T_s) - G}{1 + \beta(T_s)} \tag{3}$$

To explicitly acknowledge the dependence of R_n on T_s, $R_n(T_s)$ is defined by:

$$R_n(T_s) = R_{sn} + \varepsilon\sigma(T_s - \Delta T)^4 - \varepsilon\sigma T_s^4 \tag{4}$$

where R_{sn} is the net shortwave radiation (W m^{-2}) and is taken to be unchanged with T_s. ΔT is the temperature difference between T_s and the effective radiating temperature of the atmosphere (T_{rad}; assuming blackbody radiation, $T_{rad} = \sqrt[4]{R_{li}/\sigma}$) and is parameterized as a function of atmospheric transmissivity and geographic latitude (Yang and Roderick, 2019),

$$\Delta T = n_1 \exp(n_2\tau) + n_3 |lat| \tag{5}$$

where τ is the atmospheric transmissivity for shortwave radiation (dimensionless) and is calculated as the ratio of incoming shortwave radiation at the Earth's surface to that at the top of the atmosphere. The parameter lat is the geographic latitude (in decimal degrees), which is considered here to account for a longer pathway of short-wave radiation going through the atmosphere in higher latitudes compared to lower latitudes. n_1, n_2, and n_3 are fitting coefficients. Using extensive data over the global ocean ($n = 202,794$), Yang and Roderick (2019) determined the values of these coefficients to be $n_1=2.52$, $n_2=2.38$ and $n_3=0.035$, respectively. Here, we directly adopt these same coefficient values over land for two reasons: (i) the key processes governing the interactions between incoming and outgoing longwave radiations are essentially the same for ocean and land (mainly greenhouse gas effect), and (ii) there were many more samples available for parameterizing Eq. (5) over the ocean than that over land. Validation against observations from all 1128 non-water-limited site-days demonstrates an overall good performance of Eq. (5) in estimating ΔT over land under saturated conditions (Supplementary Figure S1).

The Bowen ratio (β) is expressed as a function of T_s:

$$\beta(T_s) = m\frac{\gamma(T_s)}{\Delta(T_s)} \tag{6}$$

where m is a fitting coefficient. γ is the psychrometric constant (kPa K^{-1}), and Δ is the slope of the saturation vapor pressure curve (kPa K^{-1}), both of which are functions of T_s:

$$\gamma(T_s) = \frac{C_P P_a}{0.622 L(T_s)} \tag{7}$$

145 $$\Delta(T_s) = \frac{4098 e_s(T_s)}{(T_s - 35.8)^2} \tag{8}$$

where C_P is the specific heat of air at constant pressure (1.01 kJ kg^{-1} K^{-1}), P_a is the air pressure (kPa), L is the latent heat of vaporization (kJ kg^{-1}), and e_s is the saturated vapor pressure (kPa).

To apply the maximum evaporation model, an array of T_s (e.g., from 250 K to 330 K at an interval of 0.1 K) is generated along with the observed R_{sn} and G and these are applied to Eq. (4) and Eq. (6) and 150 then Eq. (3) to estimate LE at each corresponding T_s. The maximum evaporation was then located in that array (see Figure 3 for an example).

3 Results

The maximum evaporation theory is tested at 86 flux sites globally, covering a wide range of bio-climates (Figure 1 and Supplementary Table S1). By pooling daily observations of H, LE and T_s across 155 all 1128 site-days, we first obtain a generic β-T_s relationship as $\beta = 0.27\gamma/\Delta$. Similarly, we also obtained a β-T_s relationship for each separate biome type as shown in Figure 1. By comparison, Yang and Roderick (2019) reported a β-T_s relationship over ocean as $\beta = 0.24\gamma/\Delta$. This means that for the same T_s, β over land is generally larger than that over ocean. Interestingly, the ocean surface β-T_s relationship is identical to that in wetlands obtained here. These β-T_s relationships will be used in the following 160 calculations of LE using the maximum evaporation approach.

To get an overview of how each of the energy fluxes varies with T_s we first examine the maximum evaporation theory using the pooled data over all 1128 site-days (Figure 3). Under this condition, the mean observed net shortwave radiation (R_{sn}) over all site-days is 176.6 W m^{-2} and G is 1.0 W m^{-2}. Since R_{sn} is not directly dependent on T_s and G is negligibly small, the term R_{sn} minus G is held constant

165   across the entire T_s range. With the increase of T_s, it is readily apparent that both outgoing and incoming

longwave radiation (R_{lo} and R_{li}) steadily increase (see Sect. 2.2 for details about the coupling between

R_{lo} and R_{li}), with R_{lo} increasing slightly faster than R_{li}, leading to a decreased net longwave radiation and

thus a decreased R_n as T_s increases (Figure 3). With this and the observed generic dependence of β on T_s

($\beta = 0.27\gamma/\Delta$, Figure 2), a maximum LE emerges along the T_s gradient that represents the interaction

170   between decreasing R_n and increasing evaporative fraction as T_s increases. For the pooled dataset used

here, the maximum LE (LE_{max}) is found to be 105.6 W m^{-2} and the corresponding T_s is 294.7 K, both of

which are very close to the averages computed from all daily flux site observations (i.e., LE_{obs} = 102.4

W m^{-2} and T_{s_obs} = 292.3 K) (Figure 3).

Having demonstrated the overall concept, we next perform the detailed calculations using data for all

175   individual site-days (Figures 4-6). Using the same generic β dependence on T_s ($\beta = 0.27\gamma/\Delta$), LE_{max}

estimated from the maximum evaporation model agrees very well with flux site observations, yielding

an R^2 of 0.92, a root-mean-squared error (RMSE) of 14.6 W m^{-2} and a mean bias of 1.6 W m^{-2} (Figure

4a). The performance of the maximum evaporation model improves slightly when the biome-specific

model parameters are used (RMSE decreases to 14.1 W m^{-2} and mean bias decreases to 1.4 W m^{-2};

180   Figure 4b). This result demonstrates that LE_{max} corresponds to the observed evaporation under well-

watered conditions across a broad range of bio-climates. In fact, when the previously identified ocean

surface β-T_s relationship is adopted, the maximum evaporation approach performs only slightly worse

than those based on the calibrated β-T_s relationship over saturated lands, yielding an R^2 of 0.91, an

RMSE of 14.8 W m^{-2} and a mean bias of 2.8 W m^{-2} (Figure 4c).

185   We next test whether the maximum evaporation approach could recover T_s over the same saturated land

surfaces. Similar to the test of LE, the three β-T_s relationships are respectively used. Results show that

when the generic β-T_s relationship over land is used (i.e., $\beta = 0.27\gamma/\Delta$), the T_s at which LE_{max} occurs

corresponds reasonably well to the observed T_s, with an R^2 of 0.62, an RMSE of 4.3 K and a mean bias

of 0.3 K (Figure 5a), indicating that the maximum evaporation approach is also able to recover T_s under

190   saturated conditions. Again, the model's performance in recovering T_s increases slightly when the

biome-specific β-T_s relationships are used (Figure 5b). When the ocean surface β-T_s relationship is used,

the model performs similarly in estimating the variability of T_s to that of the generic land β-T_s relationship (Figure 5c). However, the ocean surface β-T_s relationship (Figure 5c) results in a higher T_s mean bias compared to the β-T_s relationships obtained over land (Figure 5a).

195 Different from most state-of-the-art evaporation models, the maximum evaporation approach does not rely on observed R_n (or independent R_n estimates) as model input but estimates R_n as a result of the R_n-T_s-E interaction. Here, we also test the estimated R_n calculated using the maximum evaporation approach as the discrepancy between LE_{max} and LE_{obs} is mainly caused by the slight difference between T_{s_max} and T_{s_obs} that leads to different R_{lo} and R_{li} (and thus a different R_n) to be used in the calculation of

200 LE_{max}. It should be noted that since the observed shortwave radiation is used in the maximum evaporation model, validation of R_n is essentially the same as the validation of net longwave radiation. We find that the maximum evaporation model could satisfactorily reproduce the observed R_n when the generic land β-T_s relationship is used, as indicated by an R^2 of 0.93, an RMSE of 14.4 W m^{-2} and a mean bias of 2.3 W m^{-2} (Figure 6a). Using biome-specific β-T_s relationships or the ocean surface β-T_s

205 relationship does not considerably increase or decrease the model's performance in estimating R_n (Figures 6b and 6c).

4 Discussion

Taking R_n and/or T_s (or near-surface air temperature) to be independent forcings has long been identified as a scientific concern in the use of evaporation models (Milly, 1991; Monteith and Unsworth,

210 2013; Philip, 1987). Here, we test a maximum evaporation theory developed over the global ocean surface that addresses this concern by explicitly acknowledging the interdependence between radiation, surface temperature and evaporation (Yang and Roderick, 2019). Our new results show that there exists a maximum evaporation along the T_s gradient that corresponds to the observed evaporation under saturated conditions over land (Figures 3 and 4). In addition, the T_s at which LE_{max} occurs also

215 corresponds reasonably well to the observed T_s (Figures 3-5). These results mirror those found previously over the global ocean (Yang and Roderick, 2019). This is not a surprise since the basic principles are the same for a wet land surface and the ocean surface. These results suggest that saturated

land surfaces behave essentially the same as ocean surfaces and imply that LE_{max} is a natural attribute of the land surface when water availability does not limit evaporation. One should note that the developed

220 maximum evaporation model is only tested at the daily time scale (Figures 4-6) and longer (Figure 3). For time scales shorter than that (e.g., hourly), the diurnal cycle of E can be very different for ocean and land surfaces (Kleidon and Renner, 2017). In addition, the parameterization of the coupling between incoming and outgoing longwave radiation via Eq. 5 requires a time scale that is long enough to allow the surface heat fluxes to be fully redistributed through the atmospheric column (Yang & Roderick,

225 2019). At sub-daily scales, Eq. 5 is likely invalid because R_{lo} usually exhibits a larger diurnal range than R_{li} during a typical cloudless day (Monteith and Unsworth, 2013).

A key assumption involved in the maximum evaporation model is that β decreases with the increase of T_s under saturated conditions. Our results found this held over saturated lands but with considerable scatter (Figure 3), which may be partly caused by uncertainties in observations at flux sites.

230 Nevertheless, this key assumption has been extensively validated in previous studies based on theoretical relationships (Philip, 1987; Priestley and Taylor, 1972; Slatyer and McIlroy, 1961; Lhomme, 1997) and *in situ* observations (Andreas et al., 2013; Guo et al., 2015; Yang and Roderick, 2019; also see Supplementary Figure S2). The original maximum evaporation study reported that $\beta = 0.24\gamma/\Delta$ over global ocean surfaces (Yang and Roderick, 2019). Here, we find the generic land surface coefficient

235 increases to 0.27 (i.e., $\beta = 0.27\gamma/\Delta$, Figure 2) over vegetated lands, which indicates a slightly higher β over wet vegetated land than that over the ocean surface for the same T_s. This is biophysically reasonable, as the stoma of plant leaves represents an additional resistance to vapor transfer between the land and the atmosphere (Swann et al., 2016; Yang et al., 2019), which lowers the ability of a generic vegetated surface to convert available energy into LE for a given T_s, compared to open water surfaces.

240 In fact, our findings that one can make a reasonable estimate of LE using a generic land or ocean β-T_s relationship instead of a site-specific relationship (Figure 4) imply that R_n is the primary determinant of LE over saturated surfaces. As evaporation tends to operate at its maximum strength, sensible heat (and β) are usually very small over warm saturated land surfaces. As a result, once R_n can be accurately determined, any reasonable β-T_s relationship (Figure 2) would result in a satisfactory LE estimate

245 (Figure 5 and Supplementary Figure S3). Our result highlighted in Figure 3 shows that R_n (and hence

LE) is only a weak function of T_s and this explains why one can obtain an accurate estimate of LE using a generic β - T_s relation. However, the same logic also leads to the conclusion that an accurate β - T_s relationship will be necessary to estimate T_s, since T_s is very sensitive to changes in LE (Figure 3). In this regard, using land β - T_s relationships (preferably site-specific relations) are superior to the ocean

250 surface one (Figure 5). To further demonstrate the above points, we conduct an uncertainty test by varying the coefficient m in the β - T_s relationship in Supplementary Figure S4. We find that when m ranges from 0.18 to 0.36 (all other forcings as per Figure 3), the change in estimated LE_{max} is only 9 W m^{-2} (101.7 – 110.7 W m^{-2}), whereas the change in estimated T_{s_max} is as high as 11.6 K (287.9 – 299.5 K).

255 The ability of the maximum evaporation model to recover LE and T_s over vegetated lands under saturated conditions has an important implication for the estimation of potential evaporation (E_P), which is a central concept in hydrology and agriculture (and especially in irrigation). The underlying idea of E_P is straightforward – it is the evaporation that would occur with an unlimited supply of water. However, the formal physical definition of E_P has been widely debated in the literature (Brutsaert, 2005;

260 Donohue et al., 2010; Granger, 1989; Nash, 1989) and the calculation of E_P using conventional evaporation models is problematic (Aminzadeh et al., 2016; Roderick et al., 2015). The key scientific issue is that the meteorological forcing variables observed over actual surfaces are generally not equivalent to the meteorological variables that would be measured over a hypothetical surface with unlimited water supply. Compared with existing evaporation models, the maximum evaporation model

265 presented here requires fewer meteorological variables than existing approaches. Instead, this new approach only requires the ultimate external forcing (i.e., solar radiation), a relationship that describes a decreasing dependence of β on T_s, and a relation for incoming and outgoing longwave radiation coupling. With these, LE_{max} naturally follows from the physical interdependence between radiation, surface temperature and evaporation. These features suggest that the maximum evaporation model can

270 be used to make a strictly independent estimate of E_P. In fact, the maximum evaporation formulation directly maps to one particular definition of E_p that was proposed by Brutsaert (2015) as "the maximum evaporation that would occur over real surfaces with the actual solar forcing and a prescribed Bowen ratio".

5 Conclusions

275 In this study, we test a maximum evaporation theory that explicitly acknowledges the interdependence between radiation, surface temperature and evaporation over saturated land surfaces. Validated against flux site observations, we show that the maximum evaporation approach could recover the observed evaporation across a broad range of bioclimates. In comparison, although the model is also able to reasonably recover the observed T_s, the model's performance in recovering T_s is not as good as that for

280 LE. Nevertheless, this does not materially lead to larger errors in LE estimates, as we additionally demonstrate that LE is not sensitive to T_s changes. The overall good performance of the maximum evaporation approach over saturated surfaces implies a great potential of the method to be used for estimating potential evaporation. To calculate E_P in practice using the maximum evaporation approach, a detailed site (or biome) specific $β$-T_s relationship (e.g., Figure 2) would be favorable; otherwise, a

285 generic default $β$-T_s relationship ($β = 0.27γ/Δ$ or even $β = 0.24γ/Δ$) can also lead to a reasonable E_P estimate that remains consistent with the E_P definition by Brutsaert (2015). Supplementary Table S2 gives a worked example of applying the maximum evaporation model for E_P estimation.

Data availability

All data for this paper are properly cited and referred to in the reference list.

Author contribution

290 YY and MLR conceived the idea and designed the research. ZT performed the calculation. YY drafted the manuscript. All authors contributed to results discussion and manuscript writing.

Competing interests

The authors declare that they have no conflict of interest.

Acknowledgements

This study is financially supported by the Ministry of Science and Technology of China (Grant No. 2019YFC1510604), the National Natural Science Foundation of China (Grant No. 42041004, 42071029, 41890821) and the Guoqiang Institute of Tsinghua University (Grant No. 2019GQG1020). MLR acknowledges the support of the Australian Research Council (DP190100791). The FLUXNET community is greatly appreciated for making the eddy covariance data publicly available. The FLUXNET2015 dataset is acquired from http://fluxnet.fluxdata.org/data/fluxnet2015-dataset/.

References

Allen, R. G., Pereira, L. S., Raes, D., and Smith, M.: Crop Evapotranspiration-Guidelines for computing crop water requirements, FAO Irrigation and Drainage Paper NO. 56, Food and Agriculture Organization of the United Nations (FAO), Rome, Italy, 1998.

Aminzadeh, M., Roderick, M. L., and Or, D.: A generalized complementary relationship between actual and potential evaporation defined by a reference surface temperature, Water. Resour. Res., 52, 385–406, https://doi.org/10.1002/2015WR017969, 2016.

Andreas, E. L., Jordan, R. E., Mahrt, L., and Vickers, D.: Estimating the Bowen ratio over the open and ice-covered ocean, J. Geophys. Res. Oceans, 118, 4334–4345, https://doi.org/10.1002/jgrc.20295, 2013.

Bowen, I. S.: The ratio of heat losses by conduction and by evaporation from any water surface, Phys. Rev., 27, 779, https://doi.org/10.1103/PhysRev.27.779, 1926.

Brutsaert, W.: Hydrology: an introduction, Cambridge University Press, Cambridge, UK, 2005.

Brutsaert, W.: A generalized complementary principle with physical constraints for land-surface evaporation, Water. Resour. Res., 51, 8087–8093, https://doi.org/10.1002/2015WR017720, 2015.

Donohue, R. J., McVicar, T. R., and Roderick, M. L.: Assessing the ability of potential evaporation formulations to capture the dynamics in evaporative demand within a changing climate, J. Hydrol., 386, 186–197, https://doi.org/10.1016/j.jhydrol.2010.03.020, 2010.

320 Ershadi, A., McCabe, M. F., Evans, J. P., Chaney, N. W., and Wood, E. F.: Multi-site evaluation of terrestrial evaporation models using FLUXNET data, Agric. For. Meteorol., 187, 46–61, https://doi.org/10.1016/j.agrformet.2013.11.008, 2014.

FLUXNET: FLUXNET2015 Dataset, available at: http://fluxnet.fluxdata.org/data/fluxnet2015-dataset/ (last access: 12 November 2020), 2016.

Granger, R. J.: An examination of the concept of potential evaporation, J. Hydrol., 111, 9–19, https://doi.org/10.1016/0022-
325 1694(89)90248-5, 1989.

Guo, X., Liu, H., and Yang, K.: On the application of the Priestley–Taylor relation on sub-daily time scales, Boundary. Layer. Meteorol., 156, 489–499, https://doi.org/10.1007/s10546-015-0031-y, 2015.

Kleidon, A. and Renner, M.: An Explanation for the Different Climate Sensitivities of Land and Ocean Surfaces Based on the Diurnal Cycle, Earth Syst. Dynam., 8, 849–864, https://doi.org/10.5194/esd-8-849-2017, 2017

330 Lhomme, J. P.: A theoretical basis for the Priestley-Taylor coefficient, Boundary. Layer. Meteorol., 82, 179–191, https://doi.org/10.1023/A:1000281114105, 1997.

Maes, W. H., Gentine, P., Verhoest, N. E., and Miralles, D. G.: Potential evaporation at eddy-covariance sites across the globe, Hydrol. Earth. Syst. Sci., 23, 925–948, https://doi.org/10.5194/hess-23-925-2019, 2019.

Milly, P. C. D.: A refinement of the combination equations for evaporation, Surv. Geophys., 12, 145–154,
335 https://doi.org/10.1007/BF01903416, 1991.

Milly, P. C. D., and Dunne, K. A.: Potential evapotranspiration and continental drying, Nat. Clim. Change, 6, 946–949, http://dx.doi.org/10.1038/nclimate3046, 2016.

Monteith, J. L: Evaporation and environment, Symp. Soc. Exp. Biol., 19, 205–234, 1965.

Monteith, J. L, and Unsworth, M: Principles of environmental physics: plants, animals, and the atmosphere, Academic Press,
340 San Diego, USA, 2013.

Nash, J. E.: Potential evaporation and "the complementary relationship", J. Hydrol., 111, 1–7, https://doi.org/10.1016/0022-
1694(89)90247-3, 1989.

Pastorello, G., Trotta, C., Canfora, E., Chu, H., Christianson, D., Cheah, Y. W., et al.: The FLUXNET2015 dataset and the ONEFlux processing pipeline for eddy covariance data, Sci. Data, 7, 1–27, https://doi.org/10.1038/s41597-020-0534-3, 2020.

345   Penman, H. L.: Natural evaporation from open water, bare soil and grass, P. Roy. Soc. Lond. A., 193, 120–145, https://doi.org/10.1098/rspa.1948.0037, 1948.

Philip, J. R.: A physical bound on the Bowen ratio, J. Clim. Appl. Meteorol., 26, 1043–1045, https://doi.org/10.1175/1520-0450(1987)026<1043:APBOTB>2.0.CO;2, 1987.

Priestley, C. H. B., and Taylor, R. J.: On the assessment of surface heat flux and evaporation using large-scale parameters, 350   Mon. Weather. Rev., 100, 81–92, https://doi.org/10.1175/1520-0493(1972)100<0081:OTAOSH>2.3.CO;2, 1972.

Roderick, M. L., Greve, P., and Farquhar, G. D.: On the assessment of aridity with changes in atmospheric CO_2, Water. Resour. Res., 51, 5450–5463, https://doi.org/10.1002/2015WR017031, 2015.

Scheff, J., and Frierson, D. M. W.: Scaling potential evapotranspiration with greenhouse warming, J. Climate., 27, 1539–1558, https://doi.org/10.1175/JCLI-D-13-00233.1, 2014.

355   Schellekens, J., Dutra, E., Martinez-de la Torre, A., Balsamo, G., van Dijk, A., Weiland, F. S., Minvielle, M., Calvet, J.C., Decharme, B., Eisner, S., Fink, G., Florke, M., Pessenteiner, S., van Beek, R., Polcher, J., Beck, H., Orth, R., Calton, B., Burke, S., Dorigo, W., and Weedon, G. P.: A global water resources ensemble of hydrological models: the eartH2Observe Tier-1 dataset, Earth. Syst. Sci. Data, 9, 389–413, https://doi.org/10.5194/essd-9-389-2017, 2017.

Sheffield, J., Wood, E. F., and Roderick, M. L.: Little change in global drought over the past 60 years, Nature, 491, 435–438, 360   https://doi.org/10.1038/nature11575, 2012.

Shuttleworth, W.J.: Evaporation, in Handbook of Hydrology, chap. 4, edited by: Maidment, D. R., McGraw-Hill Education, New York, USA, 1993.

Slatyer, R.O. and McIlroy, I.C.: Practical microclimatology, Commonwealth Scientific and Industrial Research Organisation, Canberra, Australia, 1961.

365   Swann, A. L., Hoffman, F. M., Koven, C. D., and Randerson, J. T.: Plant responses to increasing CO_2 reduce estimates of climate impacts on drought severity, Proc. Natl. Acad. Sci. USA, 113, 10019–10024, https://doi.org/10.1073/pnas.1604581113, 2016.

Thornthwaite, C. W.: An approach toward a rational classification of climate, Geogr. Rev., 38, 55–94, https://doi.org/10.2307/210739, 1948.

370 Vicente-Serrano, S. M., Gouveia, C., Camarero, J. J., Beguería, S., Trigo, R., López-Moreno, J. I., Azorín-Molina, C., Pasho, E., Lorenzo-Lacruz, J., Revuelto, J., Morán-Tejeda, E., and Sanchez-Lorenzo, A.: Response of vegetation to drought time-scales across global land biomes, P. Natl. Acad. Sci. USA, 110, 52–57, https://doi.org/10.1073/pnas.1207068110, 2013.

Wang, K., and Dickinson, R. E.: A review of global terrestrial evapotranspiration: Observation, modeling, climatology, and climatic variability, Rev. Geophys., 50, RG2005, https://doi.org/10.1029/2011RG000373, 2012.

375 Yang, Y., and Roderick, M. L.: Radiation, surface temperature and evaporation over wet surfaces. Q. J. R. Meteorol. Soc., 145(720), 1118–1129, https://doi.org/10.1002/qj.3481, 2019.

Yang, Y., Roderick, M. L., Zhang, S., McVicar, T. R., and Donohue, R. J.: Hydrologic implications of vegetation response to elevated CO_2 in climate projections, Nat. Clim. Change, 9, 44–48, https://doi.org/10.1038/s41558-018-0361-0, 2019.

Figure 1. Location of the 86 flux sites used in this study. Numbers in the brackets indicate the number of sites for each biome type.
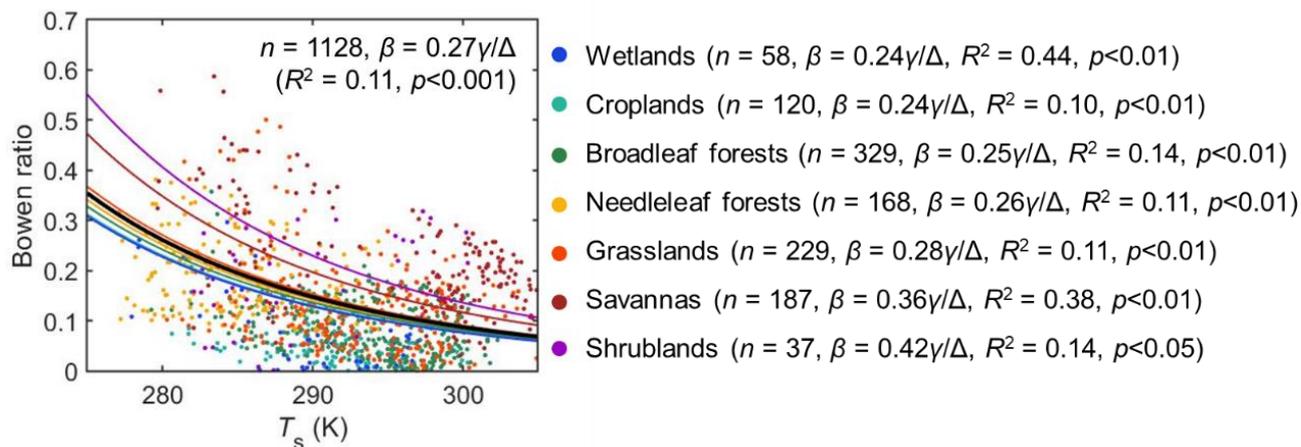
410

Figure 2. Relationship between Bowen ratio (β) and surface temperature (T_s) over saturated land surfaces. The thick black curve represents the fitted β-T_s relationship across all data points (i.e., n=1128, $\beta = 0.27\gamma/\Delta$, R^2=0.11, p<0.001), and the colored lines represent different biome types with the number of data points (n site-days) and fitted β-T_s relationship for each biome type shown in the legend.

415
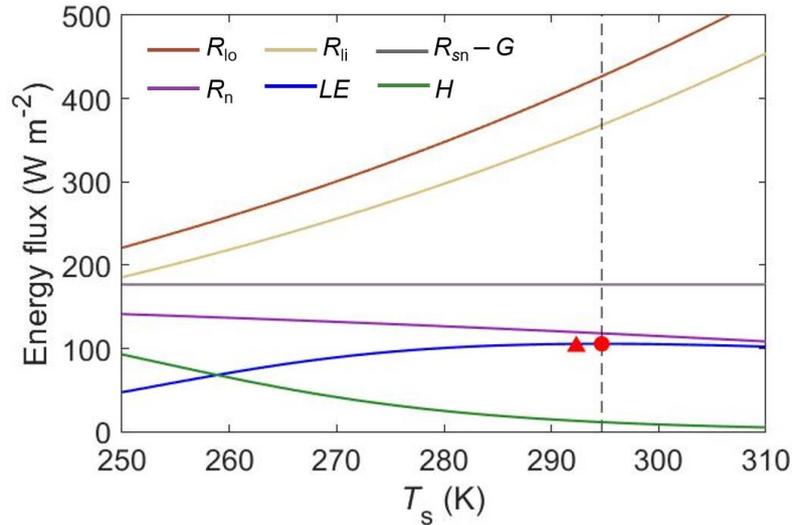
Figure 3. Variation of energy fluxes with T_s. Plot shows how the energy fluxes vary with T_s for a fixed value of $R_{sn} - G$ at 176.6 W m^{-2} (R_{sn} is the net shortwave radiation, see Eq. (4) in Sect. 2.2). The red dot indicates the maximum evaporation and the red triangle shows the observed evaporation. The T_s at which the maximum evaporation occurs is shown by the dashed vertical line.
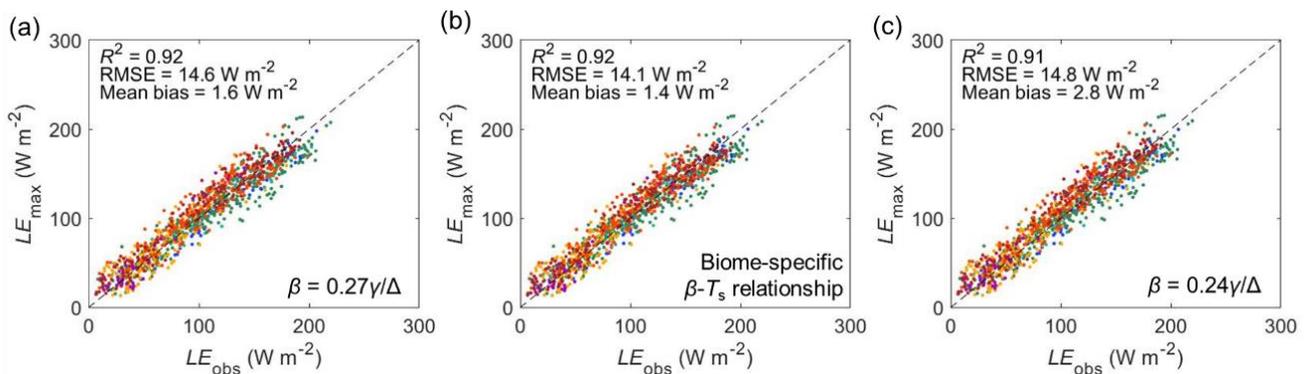
Figure 4. Comparison of the maximum evaporation and observed evaporation over saturated land surfaces using three different β-T_s relationships. (a) Generic land β-T_s relationship ($\beta = 0.27\gamma/\Delta$, $n = 1128$). (b) Biome-specific β-T_s relationships (per Figure 2). (c) Ocean surface β-T_s relationship ($\beta = 0.24\gamma/\Delta$, Yang and Roderick, 2019). The colors indicate different biome types (as provided in Figure 1). The dashed black line indicates the 1:1 line.
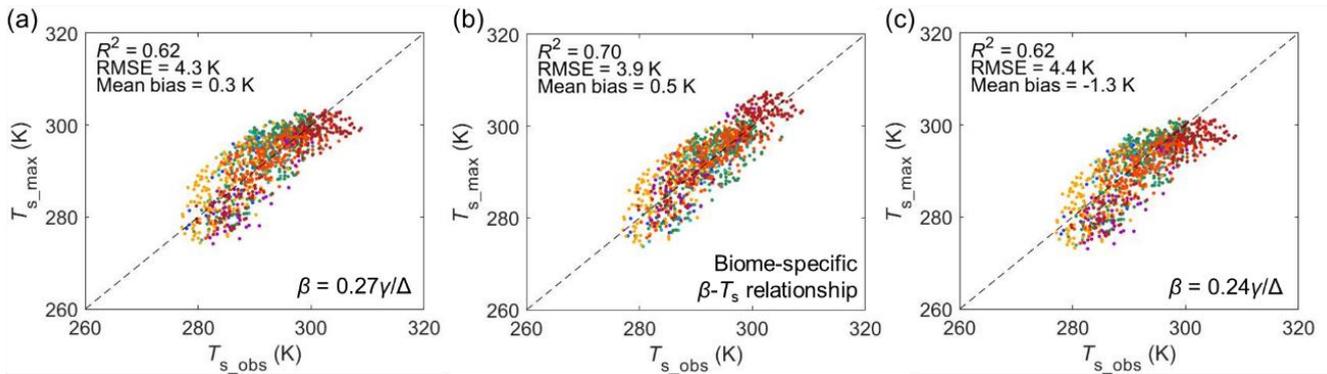
Figure 5. Comparison of the estimated and observed surface temperature over saturated land surfaces
using three different β-T_s relationships. Comparison of estimated surface temperature (T_{s_max}) with flux
site observations (T_{s_obs}). (a) Generic land β-T_s relationship ($\beta = 0.27\gamma/\Delta$, $n = 1128$). (b) Biome-specific
β-T_s relationships (per Figure 2). (c) Ocean surface β-T_s relationship ($\beta = 0.24\gamma/\Delta$, Yang and Roderick,
2019). The colors indicate different biome types (as provided in Figure 1). The dashed black line
indicates the 1:1 line.
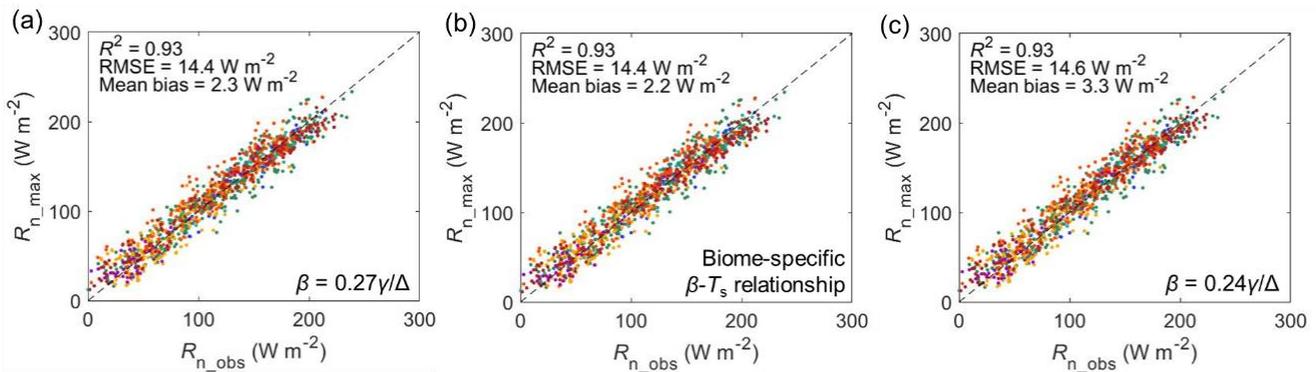
Figure 6. Comparison of the estimated and observed net radiation over saturated land surfaces using
three different β-T_s relationships. Comparison of estimated net radiation (R_{n_max}) with flux site
observations (R_{n_obs}). (a) Generic land β-T_s relationship ($\beta = 0.27\gamma/\Delta$, $n = 1128$). (b) Biome-specific β-
T_s relationships (per Figure 2). (c) Ocean surface β-T_s relationship ($\beta = 0.24\gamma/\Delta$, Yang and Roderick,
2019). The colors indicate different biome types (as provided in Figure 1). The dashed black line
indicates the 1:1 line.